Laser-cooling simulation based on the semiclassical approach

Bart Smeets, Rudolf W. Herfst, Edwin te Sligte, Peter van der Straten, Herman C. W. Beijerinck, and Karel A. H. van Leeuwen

Eindhoven University of Technology, P.O. Box 513, 5600 MB Eindhoven, The Netherlands

Received May 2, 2005; accepted June 2, 2005

We investigate the region of validity of the semiclassical approach to simulating laser cooling. We conclude that for the commonly used $\pi^x\pi^y$ polarization-gradient configuration, the semiclassical approach is valid only for transitions with recoil parameters ε_r on the order of 10^{-4} or less. For the standard laser-cooling transitions only the transitions in Rb and Cs satisfy this condition. For the Doppler and $\sigma^+\sigma^-$ polarization-gradient configuration the semiclassical approach is valid for most of the commonly used transitions; however, the expected gain in execution speed compared with quantum Monte Carlo calculations has been realized only in part. A drastic reduction in calculation time is to be expected by implementing an analytical approach to the long-term contribution of the diffusion coefficient.

OCIS codes: 020.1670, 020.7010, 140.3320.

1. INTRODUCTION

Laser cooling is a widely used technique in atomic physics. Many new fields of fundamental and applied physics, like Bose–Einstein condensation, atom interferometry, and nanofabrication by atom lithography could be explored using laser cooling to manipulate the motion of atoms, slowing and cooling them down to a few microdegrees Kelvin. To investigate atom lithography with Fe,[1,2] we want to simulate laser collimation of an Fe atomic beam.

For simulating laser cooling, a variety of approaches can be used. The most rigorous fully quantum-mechanical approaches take into account the quantum-mechanical nature of the center of mass motion as well as the random nature of spontaneous emission. These approaches are based either on the density matrix or on the Monte Carlo wave function formalism. In general, these approaches result in excellent agreement with experiments; however, they are computationally very intensive.

Simple semiclassical approaches in which the atoms are treated as classical point particles subject to averaged dipole and radiation forces derived from rate equations allow for quick calculations.[3] However, these models lack the ability to calculate more-complex laser-cooling schemes, depending on coherence between atomic states, like the $\sigma^+\sigma^-$ polarization-gradient configuration.

Nienhuis *et al.*[4] developed a semiclassical (SC) model based on an operator description in which the motion of the atoms is treated classically, but the evolution of the atomic states is governed by the optical Bloch equations (OBEs). In this approach, the motion of the atom is described by a Brownian motion due to force fluctuations resulting from the random nature of the photon recoil. For velocities $v \gg v_{\mathrm{rec}}$, with $v_{\mathrm{rec}}=\hbar k/m$ as the recoil velocity, these jumps can be neglected. The atomic velocity distribution is then governed by the Fokker–Planck equation. On the other hand, for velocities on the order of the recoil velocity, the motion of the atoms is strongly influenced by these velocity jumps. The velocity dependence of the dissipative force scales with the Doppler velocity $v_D=\Gamma/k$, with Γ as the natural linewidth and $k=2\pi/\lambda$ as the wavevector of the light. If k and Γ are such that the resulting velocity distribution is on the same order as the recoil velocity $v_{\mathrm{rec}}=\hbar k/m$, the semiclassical approach loses its validity. The recoil parameter $\varepsilon_r=v_{\mathrm{rec}}/2v_D=\hbar k^2/2m\Gamma$, which includes all the relevant atomic properties, is thus a measure of the validity of the semiclassical approach. In Table 1, a list with the commonly used atom species on which laser cooling is applied is shown. Since the recoil parameter is inversely proportional with the mass m, lighter elements can be expected to have a smaller range in which the SC model is valid. Also, elements with long-lived excited states or more energetic optical transitions are less suitable to simulate with the SC model.

A simulation was developed by Hoogerland *et al.*[5] in which atomic trajectories were calculated and the operator description of Nienhuis *et al.*[4] was used to calculate the force at each point. In this paper we describe a newly developed simulation program based on the SC approach in which the atomic motion is governed by the Fokker–Planck equation, and we investigate the influence of the recoil parameter. An existing quantum Monte Carlo (QMC) model is used to validate the resulting velocity distributions calculated with the SC model. In Section 2 the theory of both models is described. Section 3 describes the implementation of the SC model. Results are given in Section 4, followed by the conclusions in Section 5.

2. THEORY

A. Semiclassical Model

The semiclassical approach is based on the operator description of laser cooling by Nienhuis *et al.*[4] Interaction of the atoms with the light field is treated quantum mechanically and the motion of the atoms classically. During

Table 1. Recoil Parameters of the Transitions of Some of the Commonly Used Atomic Species in Experiments with Laser-Cooling Techniques

Atom	Transition	I	λ (nm)	$\Gamma\,(2\pi)$ MHz	$\varepsilon_r(10^{-3})$
^{1}H	$1\,^2S_{1/2}-2\,^2P_{3/2}$	1/2	121.57	99.58	134.5
^{4}He*	$2\,^3S_1-2\,^3P_2$		1083.33	1.62	26.2
^{4}He*	$2\,^3S_1-3\,^3P_2$		388.98	1.49	221
^{7}Li	$2\,^2S_{1/2}-2\,^2P_{3/2}$	3/2	670.96	5.92	10.7
^{23}Na	$3\,^2S_{1/2}-3\,^2P_{3/2}$	3/2	589.16	10.01	2.5
^{39}K	$4\,^2S_{1/2}-4\,^2P_{3/2}$	3/2	766.70	6.09	1.43
^{52}Cr	$a\,^7S_3-z\,^7P_4$		425.55	5.01	4.23
^{56}Fe	$a\,^5D_4-z\,^5F_5$		371.99	2.58	9.98
^{85}Rb	$5\,^2S_{1/2}-5\,^2P_{3/2}$	5/2	780.24	5.98	0.65
^{133}Cs	$6\,^2S_{1/2}-6\,^2P_{3/2}$	7/2	852.35	5.18	0.4

the cooling process the atoms undergo small velocity jumps $\hbar k/M$, where k is the wave number of the radiation and M is the atomic mass. When the final velocity distribution is much broader than such a velocity jump, the evolution of the velocity distribution $\mathcal{W}(\mathbf{v})$ is governed by the Fokker–Planck equation:

$$\frac{\partial}{\partial t}\mathcal{W}(\mathbf{v}) = -\frac{1}{M}\frac{\partial}{\partial \mathbf{v}}\cdot\mathbf{F}(\mathbf{v})\mathcal{W}(\mathbf{v}) + \frac{1}{M^2}\frac{\partial^2}{\partial \mathbf{v}\partial \mathbf{v}}:\vec{\vec{\mathbf{D}}}(\mathbf{v})\mathcal{W}(\mathbf{v}), \quad (1)$$

Here

$$\mathbf{F}(\mathbf{v}) = \langle \mathbf{f}(\mathbf{v})\rangle \quad (2)$$

is the velocity-dependent force on the atoms and $\vec{\vec{\mathbf{D}}}$ is the momentum diffusion tensor, which can be expressed as the integrated autocorrelation function of the force:

$$2\vec{\vec{\mathbf{D}}}(\mathbf{v}) = \int_0^\infty \mathrm{d}\tau[\langle \mathbf{f}(t)\mathbf{f}(t+\tau)\rangle - \langle \mathbf{f}(t)\rangle\langle \mathbf{f}(t+\tau)\rangle + \langle \mathbf{f}(t+\tau)\mathbf{f}(t)\rangle - \langle \mathbf{f}(t+\tau)\rangle\langle \mathbf{f}(t)\rangle]. \quad (3)$$

The radiation field is described by the classical electric field

$$\mathbf{E}(\mathbf{r},t) = \mathbf{E}_+(\mathbf{r})\exp(-i\omega t) + \mathbf{E}_-(\mathbf{r})\exp(i\omega t). \quad (4)$$

In the rotating-wave approximation the atom-field coupling is governed by the Rabi operator

$$\mathcal{R} = \mu_{\mathrm{eg}}\cdot\mathbf{E}_+/\hbar, \quad (5)$$

which generalizes the Rabi frequency. The internal state of the atom is described by the density matrix $\sigma(t)$ in the rotating frame. The evolution of σ is given by the OBEs:

$$\frac{\mathrm{d}\sigma_{gg}}{\mathrm{d}t} = \Gamma\sum_\beta \mathcal{Q}_\beta^\dagger\sigma_{ee}\mathcal{Q}_\beta + i\mathcal{R}^\dagger\sigma_{eg} - i\sigma_{ge}\mathcal{R},$$

$$\frac{\mathrm{d}\sigma_{ee}}{\mathrm{d}t} = -\Gamma\sigma_{ee} + i\mathcal{R}\sigma_{ge} - i\sigma_{eg}\mathcal{R}^\dagger,$$

$$\frac{\mathrm{d}\sigma_{ge}}{\mathrm{d}t} = -\left(\frac{\Gamma}{2} + i\delta\right)\sigma_{ge} + i\mathcal{R}^\dagger\sigma_{ee} - i\sigma_{gg}\mathcal{R}^\dagger,$$

$$\frac{\mathrm{d}\sigma_{eg}}{\mathrm{d}t} = -\left(\frac{\Gamma}{2} - i\delta\right)\sigma_{eg} + i\mathcal{R}\sigma_{gg} - i\sigma_{ee}\mathcal{R}, \quad (6)$$

where Γ is the spontaneous emission rate and $\delta=\omega-\omega_0$ is the detuning of the light frequency ω from the atomic resonance frequency ω_0. The operators $\mathcal{Q}_\beta$ are the dimensionless dipole operators of which the matrix elements are equal to the Clebsch–Gordan coefficients:

$$\langle eJ_em_{J_e}|\mathcal{Q}_\beta|gJ_gm_{J_g}\rangle = C_i. \quad (7)$$

The electric field and thus the Rabi operators $\mathcal{R}$ and $\mathcal{R}^\dagger$ are taken at the time-dependent position $\mathbf{r}(t)=\mathbf{r}_0+\mathbf{v}t$. This approach is justified when $|\mathbf{v}|$ is much larger than the recoil velocity $\hbar k/M$.

The velocity-dependent diffusion tensor $\vec{\vec{\mathbf{D}}}$ has two components, one due to fluctuations of the force from the driving field (stimulated term $\vec{\vec{\mathbf{D}}}_{\mathrm{st}}$) and another due to coupling of the atom to the vacuum field (spontaneous term $\vec{\vec{\mathbf{D}}}_{\mathrm{sp}}$). The spontaneous term is equal to

$$\vec{\vec{D}}_{\mathrm{sp}} = \frac{1}{2}\int \mathrm{d}\hat{n}g(\hat{\mathbf{n}})(\hbar\mathbf{k})^2\hat{\mathbf{n}}\hat{\mathbf{n}}, \quad (8)$$

where

$$g(\hat{\mathbf{n}}) = \frac{3\Gamma}{8\pi}\sum_{\hat{\mathbf{u}}\perp\hat{\mathbf{n}}} \mathrm{Tr}\hat{\mathbf{u}}^*\cdot\mathbf{Q}^\dagger\bar{\sigma}_{ee}\mathbf{Q}\cdot\hat{\mathbf{u}} \quad (9)$$

is the rate of spontaneous emission per unit solid angle in the direction of the unit vector $\hat{\mathbf{n}}$. The summation in Eq. (9) runs over two independent polarization directions $\hat{\mathbf{u}}$ orthogonal to the emission direction $\hat{\mathbf{n}}$. The bar above σ_{ee} refers to a steady-state situation. The vector operator $\mathbf{Q}$ has three components that in Cartesian coordinates are

$$\mathcal{Q}_x = \frac{-1}{\sqrt{2}}(\mathcal{Q}_1 - \mathcal{Q}_{-1}), \quad \mathcal{Q}_y = \frac{-1}{i\sqrt{2}}(\mathcal{Q}_1 + \mathcal{Q}_{-1}), \quad \mathcal{Q}_z = \mathcal{Q}_0. \quad (10)$$

The force operator resulting from the driving field is given by $\mathbf{f}^{\mathrm{st}}=\hbar(\nabla\mathcal{R}+\nabla\mathcal{R}^\dagger)$. To calculate the stimulated term ($\vec{D}_{\mathrm{st}}$) it is convenient to introduce the evolution operator $U(t+\tau,t)$, which is defined by

$$\sigma(t+\tau) = U(t+\tau,t)\sigma(t). \quad (11)$$

This means that at a given time t the operator $U(t+\tau,t)$ takes the argument and uses the OBE to calculate its value of it at $t+\tau$. With this convention the correlation functions are equal to

$$\langle \mathbf{f}^{\mathrm{st}}(t)\mathbf{f}^{\mathrm{st}}(t+\tau)\rangle = \mathrm{Tr}U(t+\tau)[\bar{\sigma}(t)\mathbf{f}^{\mathrm{st}}(t)]\mathbf{f}^{\mathrm{st}}(t+\tau), \quad (12)$$

$$\langle \mathbf{f}^{\mathrm{st}}(t+\tau)\mathbf{f}^{\mathrm{st}}(t)\rangle = \mathrm{Tr}\mathbf{f}^{\mathrm{st}}(t+\tau)U(t+\tau)[\mathbf{f}^{\mathrm{st}}(t)\bar{\sigma}(t)]. \quad (13)$$

From Eq. (3) the stimulated diffusion can be calculated using these correlation functions.

B. Quantum Monte-Carlo Model

The QMC model is based on Mollow's treatment of resonant light scattering.[6] A detailed description of the model for arbitrary light fields is given by Dum *et al.*[7] What fol-

lows is a summary of the important features. The numerical implementation of the QMC model is described by Hoogerland *et al.*[5] In contrast with the SC model the kinetic energy is included in the Hamiltonian, which implies that the wave function describes not only the internal states of the atom but also its center-of-mass motion. For an atom in a light field, the total Hamiltonian $\hat{H}$ is given by

$$\hat{H} = \frac{\hat{p}^2}{2M} + \hat{H}_{0A} + \hat{H}_{0F} + \hat{H}_I(t), \tag{14}$$

where $\hat{p}$ is the momentum of the atom and M is the mass. The operator $\hat{H}_{0A} = \hbar\omega_{eg}\hat{a}^\dagger\hat{a}$ is the Hamiltonian of the free atom, where $\hat{a} = |g\rangle\langle e|$ and $\hat{a}^\dagger = |e\rangle\langle g|$ are the atomic lowering and raising operators, respectively. The kets $|g\rangle$ and $|e\rangle$ are the time-independent ground and excited states, respectively. The operator $\hat{H}_{0F}$ represents the Hamiltonian of the radiation field. In the dipole approximation the interaction Hamiltonian $\hat{H}_I$ is given by

$$\hat{H}_I(t) = -\mu_{\mathrm{eg}}^{*} \cdot \hat{\mathbf{E}}^\dagger\hat{a} + \mathrm{H.C.} \tag{15}$$

where μ_{eg} is the atomic dipole matrix, $\hat{\mathbf{E}}$ is the electric field operator, and H.C. is the Hermitian conjugate. The laser light field can be represented by a complex vector $\varepsilon_c(\mathbf{r},t)$, which is for a plane wave in the z direction $\varepsilon_c(z,t) = \varepsilon_0 \exp[i(kz - \omega t)]$. At the start ($t=0$) we assume all modes of the light field are empty except the laser mode. We expand the full wave function of atoms and light field $\Psi(\mathbf{r},t)$ in partial wave functions $\Psi^n(\mathbf{r},t)$ each with n spontaneously emitted photons:

$$\Psi(\mathbf{r},t) = \Psi^0(\mathbf{r},t) + \sum_{n=1}^{\infty} \Psi^n(\mathbf{r},t). \tag{16}$$

For the partial wave function $\Psi^0(\mathbf{r},t) = C_g^0(\mathbf{r},t)|g,\{0\}\rangle + C_e^0(\mathbf{r},t)|e,\{0\}\rangle$ a set of Schrödinger-like equations can be derived. The modulus $|\Psi^0(t)|^2 = |C_g^0(t)|^2 + |C_e^0(t)|^2$ is the probability that no spontaneous emissions have occurred until time t. The loss of probability $1 - |\Psi^0(t)|^2$ is equal to the photon waiting-time distribution $W(t)$, which is given by

$$1 - |\Psi^0(t)|^2 = \int_0^t W(t')\mathrm{d}t' = \Gamma \int_0^t |C_e^0(t')|^2 \mathrm{d}t'. \tag{17}$$

In a Monte Carlo simulation this photon waiting-time distribution can be used to calculate the time at which a photon is spontaneously emitted by picking a random number $\Upsilon \in [0,1]$ and solving the equation

$$1 - |\Psi^0(t)|^2 = \Upsilon. \tag{18}$$

At this moment the model assumes no further interaction with the spontaneously emitted photon, and the atom starts over in the zero-photon ground state with C_g^0 normalized to 1 and all other C terms are zero. In the case of a two-level atom in a traveling-wave laser field, the complete time evolution of the coefficients C_g^0 and C_e^0 is as given by Mollow[6]; it has been applied to a Monte Carlo simulation of cooling processes[8,9] and generalized by Dum *et al.*[7] and Dalibard *et al.*[10] to an arbitrary light field and magnetic atomic substructure.

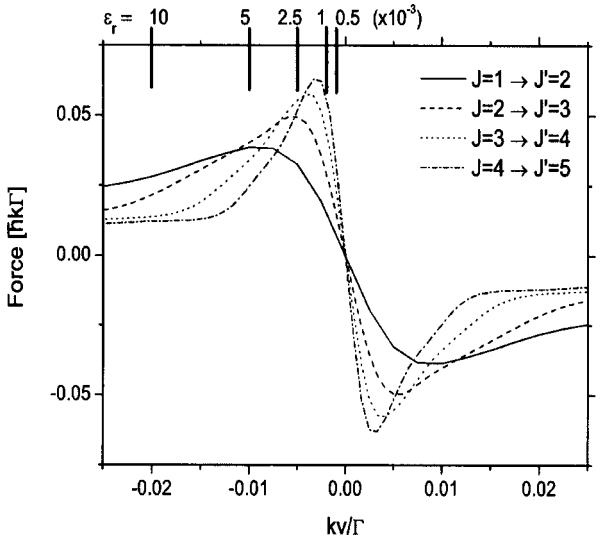

Fig. 1. Sub-Doppler force for different J values in the crossed linear-polarization configuration, calculated with the SC method. The saturation parameter is $s=2$, and detuning is $\delta=-2\Gamma$.

The momentum in the direction of the laser field is treated quantum mechanically with operator $\hat{p}$ and eigenstates $|p\rangle$. The motion perpendicular to the laser field is treated classically. To include magnetic substructure, the partial wave function Ψ^0 is expanded in time-independent states $|\alpha, m_\alpha\rangle$, and the product wave function is represented by $|\alpha, m_\alpha, p\rangle$, with $\alpha = e, g$. If there is no spontaneous emission, the atomic momentum is quantized as $|p_0 + j\hbar k\rangle$ with $p_0 = \hbar k_0$ as the initial momentum and j as an integer, with j even or odd for the ground states or excited states, respectively. We now have a family F_{p_0} of states that are internally coupled only by stimulated processes. The states of this family are denoted by $|\alpha, m_\alpha, j\rangle$ and have coefficients $C^j_{\alpha m_\alpha}$. Spontaneous emission will transfer an atom to another family $F_{p_0'}$.

The equations of motion for the coefficients $C^j_{\alpha m_\alpha}(t)$ for a family with initial momentum $p_0 = \hbar k_0$ are in a one-dimensional laser configuration in the z direction given by

$$\begin{aligned} i\hbar \frac{\mathrm{d}}{\mathrm{d}t} C^j_{gm_g}(t) = & \left[\frac{\hbar^2}{2M}(jk + k_0)^2 \right] C^j_{gm_g}(t) \\ & + \sum_{q=\pm 1} \frac{\hbar\Omega^{*}_{eg}}{2} \langle j_g m_g 1q | j_e (m_g - q) \rangle [\epsilon_q^{+*} C^{j+1}_{e(m_g - q)}(t) \\ & + \epsilon_q^{-*} C^{j-1}_{e(m_g - q)}(t)], \end{aligned} \tag{19}$$

$$\begin{aligned} i\hbar \frac{\mathrm{d}}{\mathrm{d}t} C^j_{em_e}(t) = & \left[\frac{\hbar^2}{2M}(jk + k_0)^2 - \hbar(\Delta + i\Gamma/2) \right] C^j_{em_e}(t) \\ & + \sum_{q=\pm 1} \frac{\hbar\Omega_{eg}}{2} \langle j_g (m_e + q) 1q | j_e (m_e) \rangle [\epsilon_q^{+} C^{j-1}_{g(m_e + q)}(t) \\ & + \epsilon_q^{-} C^{j+1}_{g(m_e + q)}(t)]. \end{aligned} \tag{20}$$

The Rabi frequency $\Omega_{eg} = \Gamma_{eg}[I/(2I_0)]^{1/2}$ with I_0 as the saturation intensity. The relative strengths of the or-

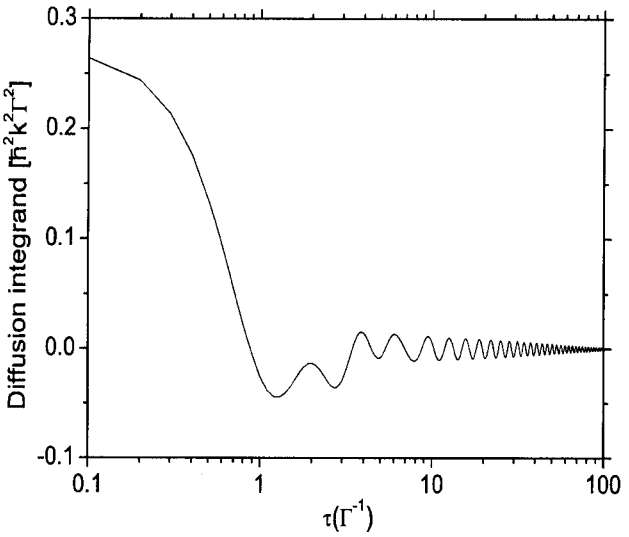

Fig. 2. Integrand of the stimulated part of the diffusion coefficient for $J=1\rightarrow J'=2$. The part due to a spontaneous decay of the excited state decays on a timescale of $\Gamma-1$. The part due to a pumping over the ground-state sublevels decays on a timescale of 100 $\Gamma-1$. The decay rate of the latter part will decrease with $[J(J+1)]-1$. The transverse velocity in this particular case is $v=\Gamma/k$.

thogonal circular polarization components +1 and −1 of the individual laser beams in the + and − directions are denoted by $\epsilon_{\pm 1}^{\pm}$.

3. IMPLEMENTATION OF THE SEMICLASSICAL MODEL

The velocity dependent force is calculated by first assuming a constant velocity. The density matrix evolves according to Eq. (6), until steady state is reached. Then $\mathrm{Tr}(\sigma\mathbf{f})$ is evaluated and averaged while the atom moves over one wavelength. In Fig. 1 the calculated force is shown for different J values in a crossed linear polarization configuration ($\pi^x\pi^y$). The maximum force increases with larger J values and the slope of the force becomes steeper, resulting in stronger damping, but it acts on a smaller velocity range compared with smaller J values.

The diffusion coefficient is calculated by evaluating the integral of Eq. (3) for different velocities. The spontaneous and stimulated parts are calculated separately. The averaging over a wavelength of the spontaneous part proceeds in the same way as the force. For the stimulated part the integrand is first evaluated with $\langle\mathbf{f}^{\mathrm{st}}(t+\tau)\rangle=\mathrm{Tr}\,U(t+\tau)\times[\sigma(t)]\mathbf{f}^{\mathrm{st}}(t+\tau)$. Since the evolution of the autocorrelation uses the same differential equations as the density matrix,[4] the timescale on which the diffusion coefficient converges is the same as the timescale to reach a steady state for the density matrix. The integrand of the stimulated part of the diffusion coefficient in a $\pi^x\pi^y$ configuration is shown in Fig. 2. The rapidly decaying part on the timescale of Γ^{-1} is a result of the spontaneous decay of the excited state. The slowly decaying part is the contribution from the optical pumping rate i.e., the rate of transfer between the lower-level magnetic substates. This pumping rate decreases with $[J(J+1)]^{-1}$, resulting in a proportionally longer calculation time for higher J values and in decay times longer than the interaction time when the laser cooling of atomic beams is simulated. After integration the stimulated part of the diffusion coefficient is averaged over a wavelength by choosing several transversal positions within a wavelength for $\bar{\sigma}(t)$. In Fig. 3 the stimulated and spontaneous parts of the diffusion coefficient are shown for a $\pi^x\pi^y$ polarization configuration and for a $J=1\rightarrow J'=2$ transition. Empirically, we observe that the diffusion coefficient does not deviate more than 0.2% between calculations with different transverse positions when the number of positions over which the diffusion efficient is averaged is at least 16.

The force and diffusion coefficient scale with $\hbar k\Gamma$ and $(\hbar k)^2\Gamma$, respectively. We can use the following transformation: $t'=\Gamma t$, $v'=kv_z/\Gamma$, $\mathcal{F}=\vec{F}_z/(\hbar k\Gamma)$, and $\mathcal{D}=\vec{\vec{D}}_{zz}/(\hbar^2k^2\Gamma)$. The dimensionless Fokker–Planck equation then becomes

$$\frac{\partial}{\partial t'}W(v',t')=-2\varepsilon_r\frac{\partial}{\partial v'}\mathcal{F}(v')W(v',t')+4\varepsilon_r^2\frac{\partial^2}{\partial v'^2}\mathcal{D}(v')W(v',t'). \tag{21}$$

The Fokker–Planck equation now scales with ε_r. The larger the recoil parameter is, the more dominant the diffusion will be in the cooling process. All the simulations are initialized with a flat velocity distribution.

4. RESULTS

In Fig. 1 the recoil velocity is indicated for different recoil parameters ε_r. For most of the $\pi^x\pi^y$ sub-Doppler force profiles, the capture velocity is on the same order as the recoil velocity. In that range the validity of the SC model is questionable. To investigate this effect the velocity distributions obtained with the SC calculations are compared with the distributions resulting from the QMC model. All distributions are calculated with a $J=1\rightarrow J'=2$ transition to limit the calculation time to approximately 3 h on a Pentium 4 2 GHz computer for both mod-

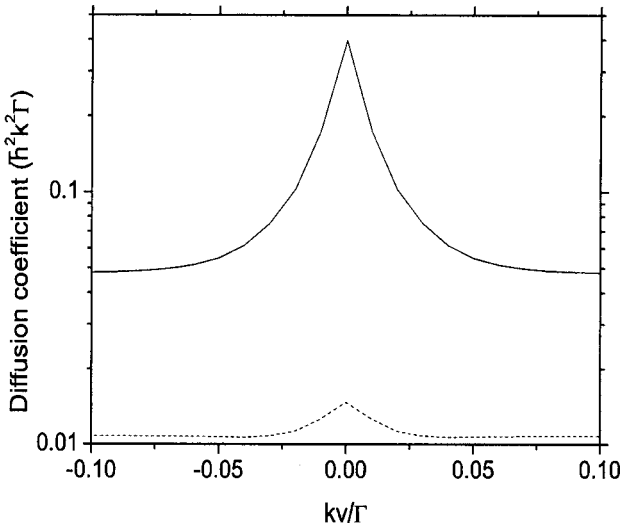

Fig. 3. Stimulated (solid curve) and spontaneous (dotted curve) part of the diffusion coefficient for crossed linear polarizations for a saturation parameter $s=2$ and a detuning $\delta=-2\Gamma$.

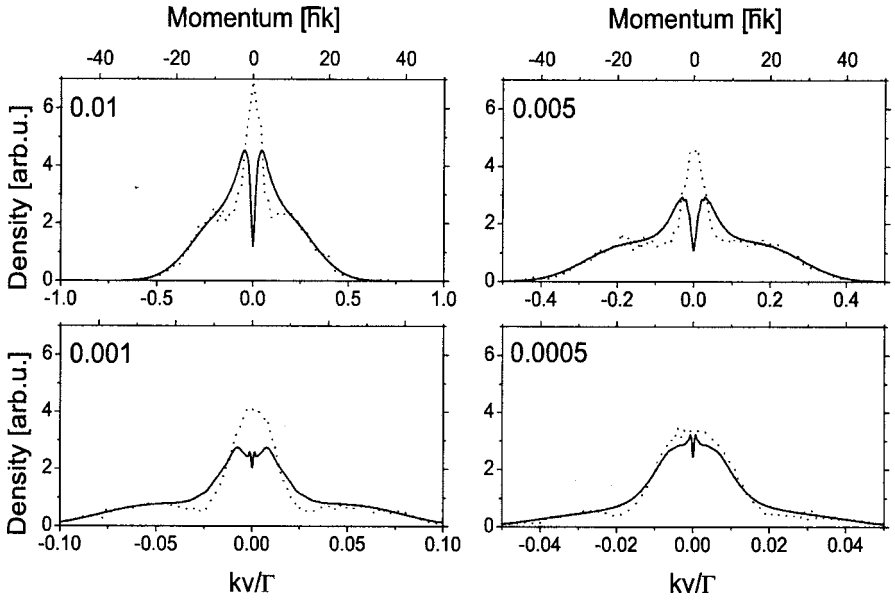

Fig. 4. Velocity distributions for different recoil parameters $\epsilon r = \hbar k 2/2m\Gamma = 0.01$ down to 0.0005 as indicated in the figure, with saturation parameter $s=2$ and detuning $\delta=-2\Gamma$ for a $J=1\rightarrow J'=2$ transition. The solid curves are the SC data; the dotted curves are the QMC data.

els. The distributions are shown in Fig. 4. Each of the distributions consists of a broad background that is the Doppler-cooled part and a peak on top that is the sub-Doppler-cooled part. With decreasing recoil parameter the distributions of both models show better resemblance. The SC distributions show a dip in the middle of the distribution that becomes sharper and deeper when the recoil parameter is increased. With larger recoil parameters, the diffusion coefficient becomes dominant in the Fokker–Planck equation. The sharp peak in the diffusion coefficient near $v=0$ for a $\pi^x\pi^y$ polarization configuration as shown in Fig. 3 results in the dip in the middle of the velocity distribution, where the force is smaller. One could think of expanding the Fokker–Planck equation to higher-order terms. At these high recoil parameters, the contribution of a third-order term that scales with ε_r^3, will not be negligible and will balance the high diffusion near $v=0$. This would solve the problem of the dip in the velocity distribution. However, at these large recoil parameters, the recoil velocity becomes important, resulting in incorrect distributions even with the inclusion of higher-order terms, since the velocity range where the sub-Doppler force is active will then be on the order of the recoil velocity. Larger J values will further decrease the validity range, since the force acts on even smaller velocity ranges (Fig. 1). A small, very sharp feature is present at recoil parameters $\varepsilon_r=0.001$ and 0.0005. This is due to a numerical artifact of the calculation near $v=0$. At these low velocities the force is very weak, and even small numerical errors in the calculation of the force near $v=0$ show up in the final distribution.

The Doppler-cooled part of both velocity distributions shows striking resemblance. The velocity range on which the Doppler force acts is much larger than the recoil velocity, and the corresponding diffusion coefficient is low enough for the Fokker–Planck equation to be valid for all the recoil parameters in Fig. 4.

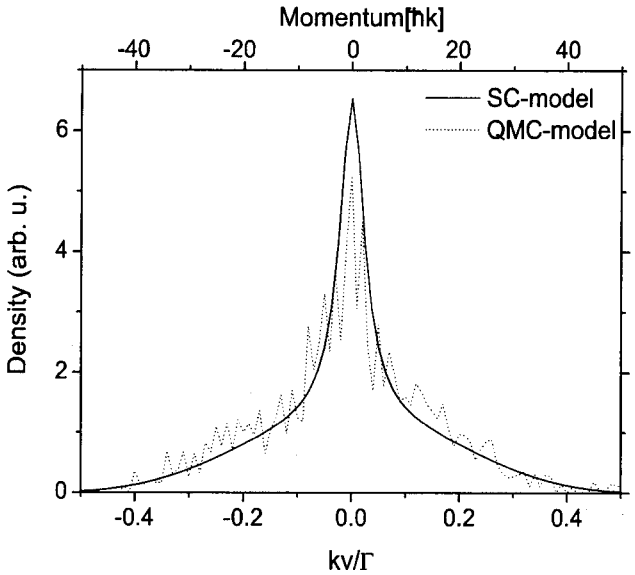

Fig. 5. Velocity distribution for the $\sigma^+\sigma^-$ configuration. Saturation parameters is $s=2$, detuning is $\delta=-2\Gamma$, and recoil parameter is $\epsilon=0.005$.

For the elements in Table 1, only Cs and Rb have low-enough recoil parameters to simulate a crossed linear polarization configuration without showing a dip in the middle of the resulting velocity distribution. However, for these alkali atoms hyperfine splitting should be included, which for Cs and Rb implies transitions with F values larger than 1, reducing the allowed velocity range.

In Fig. 5 the velocity distributions for a $\sigma^+\sigma^-$ configuration with $\varepsilon_r=0.005$ of both models are shown. The match between both models is better than in the equivalent situation in the crossed linear polarization case. The dip in the middle of the SC distributions due to imbalance between force and diffusion in the Fokker–Planck equation is absent owing to a much-lower diffusion, as shown in

Fig. 6. Also, the damping is weaker and the capture velocity is larger at the same laser settings. The capture velocity of the $\sigma^+\sigma^-$ force is much larger than the recoil velocity. For this situation, the SC distribution is much smoother than the QMC distribution for equal computation time. This implies that the QMC simulation should be executed with more atoms to obtain better statistics, which puts the SC simulation in an advantage regarding the computation time for the $\sigma^+\sigma^-$ case.

5. CONCLUDING REMARKS

Laser cooling is simulated by a newly developed simulation based on a SC approach. Intrinsically, this method has the potential of being much faster than an existing QMC model. At this stage this potential is only realized for the $\sigma^+\sigma^-$ configuration. However, in order to save drastically on calculation time for both $\sigma^+\sigma^-$ and $\pi^x\pi^y$ polarization configurations, the slowly decaying part of the diffusion integrand can be very well approximated analytically by a decaying sine of the form $A=\exp(-\gamma t)\sin(\beta t+\phi)$. This can be analytically integrated to $(\beta\cos\phi+\gamma\sin\phi)/(\beta^2+\gamma^2)$. The analytical approximation could be very useful especially for simulation of laser cooling of transitions with large J values. We estimate a twentyfold improvement in calculation time for a $J=1\rightarrow J'=2$ transition and even a hundredfold improvement for a $J=4\rightarrow J'=5$ transition when this approximation is used.

For simulations of the $\pi^x\pi^y$ configuration the SC model gives comparable results with respect to the QMC model only for low recoil parameters. For high recoil parameters there are two problems: The Fokker–Planck equation should be expanded to higher-order terms and the SC approach, which does not take the recoil velocity into account, is not sufficient, since the velocity range on which the sub-Doppler-cooling force acts, becomes on the order of the recoil velocity.

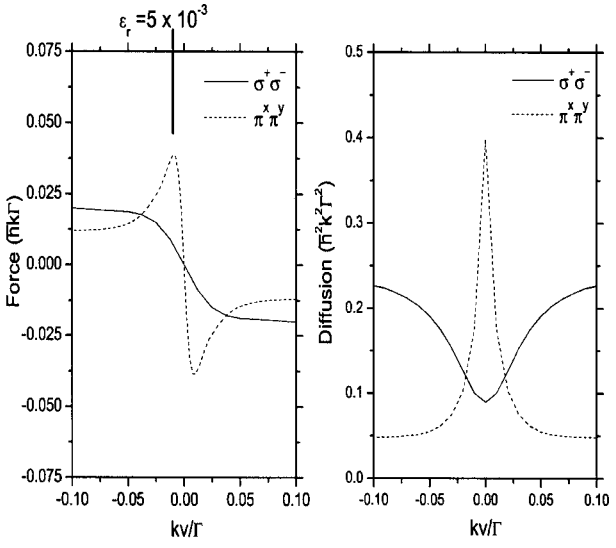

Fig. 6. Force and diffusion profile for $\pi^x\pi^y$ and $\sigma^+\sigma^-$ configurations. The recoil velocity for this particular recoil parameter is indicated.

Of the most commonly used atomic species in laser cooling experiments, only Rb and Cs have low-enough recoil parameters to be able to simulate a crossed linear polarization configuration ($\pi^x\pi^y$) with the SC approach.

Owing to the much-lower diffusion coefficient near $v=0$ for the $\sigma^+\sigma^-$ polarization configuration compared with the $\pi^x\pi^y$ configuration, the SC model is valid for much larger recoil parameters. In the $\sigma^+\sigma^-$ configuration the SC model results in smoother distributions compared with the QMC model for equal calculation times. For Doppler cooling both models give equal results over a wide recoil parameter range.

In conclusion, the simulation based on the SC approach of Nienhuis *et al.*[4] can be used to simulate laser cooling for Doppler cooling and in the $\sigma^+\sigma^-$ configuration over a wide recoil parameter range, with a calculation time advantage over a full QMC model. For the $\pi^x\pi^y$ polarization configuration this simulation gives comparable results with the QMC model only when recoil parameters are on the order of 10^{-4} or less.

ACKNOWLEDGMENTS

This work is financially supported by the Dutch Foundation for Fundamental Research on Matter. The authors thank E. D. J. Vredenbregt for his work on the QMC simulation.

REFERENCES

1. E. te Sligte, B. Smeets, K. M. R. van der Stam, R. W. Herfst, P. van der Straten, H. C. W. Beijerinck, and K. A. H. van Leeuwen, "Atom lithography of Fe," Appl. Phys. Lett. **85**, 4493–4495 (2004).
2. G. Myszkiewicz, J. Hohlfeld, A. J. Toonen, A. F. Van Etteger, O. I. Shklyarevskii, W. L. Meerts, Th. Rasing, and E. Jurdik, "Laser manipulation of iron for nanofabrication," Appl. Phys. Lett. **85**, 3842–3844 (2004).
3. E. J. D. Vredenbregt and K. A. H. van Leeuwen, "Laser cooling and trapping visualized," Am. J. Phys. **71**, 760–765 (2003).
4. G. Nienhuis, P. van der Straten, and S.-Q. Shang, "Operator description of laser cooling below the Doppler limit," Phys. Rev. A **44**, 462–474 (1991).
5. M. D. Hoogerland, H. F. P. de Bie, H. C. W. Beijerinck, E. J. D. Vredenbregt, K. A. H. van Leeuwen, P. van der Straten, and H. J. Metcalf, "Force, diffusion, and channeling in sub-Doppler laser cooling," Phys. Rev. A **54**, 3206–3218 (1996).
6. B. R. Mollow, "Pure-state analysis of resonant light scattering: radiative damping, saturation, and multiphoton effects," Phys. Rev. A **12**, 1919–1943 (1975).
7. R. Dum, P. Zoller, and H. Ritsch, "Monte Carlo simulation of the atomic master equation for spontaneous emission," Phys. Rev. A **45**, 4879–4887 (1992).
8. R. Blatt, W. Ertmer, P. Zoller, and J. L. Hall, "Atomic-beam cooling: a simulation approach," Phys. Rev. A **34**, 3022–3033 (1986).
9. M. D. Hoogerland, M. N. H. Wijnands, H. J. Senhorst, H. C. W. Beijerinck, and K. A. H. van Leeuwen, "Photon statistics in resonance fluorescence: Results from an atomic-beam deflection experiment," Phys. Rev. Lett. **65**, 1559–1562 (1990).
10. J. Dalibard, Y. Castin, and K. Mølmer, "Wave-function approach to dissipative processes in quantum optics," Phys. Rev. Lett. **68**, 580–583 (1992).